



Published in final edited form as:

Nat Genet. 2020 November ; 52(11): 1208–1218. doi:10.1038/s41588-020-00726-6.

Pan-cancer single cell RNA-seq uncovers recurring programs of cellular heterogeneity

Gabriela S. Kinker^{*,1,4}, Alissa C. Greenwald^{*,1}, Rotem Tal¹, Zhanna Orlova¹, Michael S. Cuoco², James M. McFarland³, Allison Warren³, Christopher Rodman², Jennifer A. Roth³, Samantha A. Bender³, Bhavna Kumar⁵, James W. Rocco⁵, Pedro ACM Fernandes⁴, Christopher C. Mader³, Hadas Keren-Shaul^{6,7}, Alexander Plotnikov⁶, Haim Barr⁶, Aviad Tsherniak³, Orit Rozenblatt-Rosen², Valery Krizhanovsky¹, Sidharth V. Puram⁸, Aviv Regev², Itay Tirosh^{1,#}

¹Dept. of Molecular Cell Biology, Weizmann Institute of Science, Rehovot, Israel

²Klarman Cell Observatory, Broad Institute of MIT and Harvard, Cambridge, MA, USA

³Cancer Program, Broad Institute of MIT and Harvard, Cambridge, MA, USA

⁴Institute of Bioscience, University of Sao Paulo, Sao Paulo, Brazil

⁵Dep. of Otolaryngology-HNS, The Ohio State University Wexner Medical Center, Columbus, OH, USA

⁶The Nancy & Stephen Grand Israel National Center for Personalized Medicine, Weizmann Institute of Science, Rehovot, Israel

⁷Life Science Core Facility, Weizmann Institute of Science, Rehovot, Israel

⁸Department of Otolaryngology, Washington University School of Medicine, St. Louis, USA

Abstract

Cultured cell lines are the workhorse of cancer research, but it is unclear to what extent they recapitulate the cellular heterogeneity observed among malignant cells in tumors. To address this, we used multiplexed single cell RNA-seq to profile ~200 cancer cell lines from 22 cancer types. We uncovered 12 expression programs that are recurrently heterogeneous within many cancer cell lines. These programs are associated with diverse biological processes including cell cycle, senescence, stress and interferon responses, epithelial-mesenchymal transition, and protein maturation and degradation. Notably, most of these recurrent programs of heterogeneity recapitulate those recently observed within human tumors. The similarity to tumors allowed us to prioritize specific cell lines as model systems of cellular heterogeneity. We used two such models

#corresponding author: itay.tirosh@weizmann.ac.il.

*Equal co-authors

Code availability

R code for performing the analyses described here is available at https://github.com/gabrielakinker/CCLC_heterogeneity and upon request from the corresponding author.

Competing interests

A.R. is a founder and equity holder of Celsius Therapeutics and a SAB member of Neogene Therapeutics, ThermoFisher Scientific and Syros Pharmaceuticals.

to demonstrate the regulation and dynamics of an epithelial senescence-related program that is observed in subpopulations of cells within cell lines and tumors. We further demonstrate unique drug responses of these subpopulations, highlighting their potential clinical significance. Our work describes the landscape of cellular heterogeneity within diverse cancer cell lines, and identifies recurrent patterns of heterogeneity that are shared between tumors and specific cell lines.

Cellular plasticity and heterogeneity are fundamental features of human tumors that play a major role in disease progression and treatment failure^{1,2}. For example, rare subpopulations of tumor cells may underlie resistance to treatments or facilitate metastasis. Single-cell RNA sequencing (scRNA-seq) has emerged as a valuable tool to study the heterogeneity within tumors³⁻¹². Initial scRNA-seq studies defined the expression patterns of intra-tumoral heterogeneity (ITH), yet their mechanisms and functional implications were difficult to resolve, calling for extensive follow up studies in model systems.

In principle, genetic diversity, epigenetic plasticity, and interactions within the tumor microenvironment all contribute to the heterogeneity observed across malignant cells. However, we hypothesize that a considerable fraction of the ITH expression patterns reflect intrinsic cellular plasticity that exists even in the absence of genetic diversity and a native microenvironment. For example, we previously reported an epithelial-to-mesenchymal transition (EMT)-like program in head and neck squamous cell carcinoma (HNSCC) that was partially preserved in one of a few tested cell lines⁵. Similarly, drug resistance programs identified in tumors were recapitulated and studied in melanoma cell lines^{6,13,14}. Additionally, the existence of phenotypic diversity within cancer cell lines has been established for many years, but often in a highly context-specific manner and without a direct link back to *in vivo* patterns of diversity¹⁵⁻¹⁸. To further examine the ability of cancer cell lines to recapitulate ITH programs, we sought to define the landscape of cellular diversity within a large number of cell lines from the Cancer Cell Line Encyclopedia (CCLE) collection^{19,20}.

Pan-cancer scRNA-seq of human cell lines

We developed and applied a multiplexing strategy where cells from different cell lines are profiled in pools by scRNA-seq and then computationally assigned to the corresponding cell line (Fig. 1A). We utilized existing pools that were previously generated from the CCLE collection^{19,21}. Each pool consisted of 24-27 cell lines from diverse lineages but with comparable proliferation rates, and was profiled by scRNA-seq with the 10x Genomics Chromium system, for an average of 280 cells per cell line (Methods). We profiled eight CCLE pools, along with one smaller custom pool that included HNSCC cell lines.

We assigned profiled cells to cell lines based on consensus between two complementary approaches, using genetic and expression profiles (Fig. 1A). First, cells were clustered by their global expression profile, and each cluster was mapped to the cell line with the most similar bulk RNA-seq profile²⁰. Second, by detection of single nucleotide polymorphisms (SNPs) in the scRNA-seq reads, we assigned cells to the cell line with highest similarity by SNP profiles derived from bulk RNA-seq^{20,22}. Cell line assignments based on gene expression and SNPs were consistent for 98% of the cells, which were retained for further

analysis (e.g. Fig. 1B). The few inconsistent assignments were observed primarily in cells with low data quality, resulting in low SNP coverage, which were therefore excluded. Cell lines with less than 50 assigned cells were also excluded from further analyses, as were low-quality cells and suspected doublets. Overall, following assignment and quality control filters, we studied the expression profiles of 53,513 cells, from 198 cell lines (56-1,990 cells per cell line; fig. S1A), reflecting 22 cancer types (Fig. 1C; Table S1). We detected an average of 19,264 UMIs and 3,802 genes per cell, underscoring the high quality of our dataset (fig. S1A).

A potential caveat of our multiplexing approach is that in the previously generated CCLE pools, but not in the custom HNSCC pool, cell lines were co-cultured for 3 days prior to profiling by scRNA-seq and hence their expression patterns may have been affected. However, our analyses suggest a limited effect of co-culturing, particularly when considering the heterogeneity within each cell line, which is our focus in this work. First, the patterns of heterogeneity were as similar between cell lines from the same pool as between cell lines of different pools (fig. S1B). Second, we performed a control experiment in which six cell lines were profiled with and without co-culturing for 3 days. Co-culturing had a modest effect on average gene expression in each cell line, while patterns of heterogeneity were highly consistent between the two conditions (fig. S1C–F).

Discrete and continuous patterns of expression heterogeneity within cell lines

Extensive variability of gene expression was identified across cells within individual cell lines, including discrete subpopulations of cells, as well as continuous patterns that reflect spectra of cellular states (Fig. 2A). To identify discrete subpopulations we used dimensionality reduction with t-Distributed Stochastic Neighbor Embedding (t-SNE) followed by density-based clustering (DBSCAN; fig. S2A; Methods). Discrete clusters of cells within a cell line were found only for a minority (11%) of the cell lines: three cell lines had three or more clusters, three had two clusters of comparable sizes, and 16 had one major and one minor cluster (Fig. 2B and S2B). For each such cluster, we identified the top 50 upregulated genes compared to all other cells from the same cell line (Table S2). These expression programs showed limited similarities to one another, both within cell lines of the same cancer type and across different cancer types, indicating that discrete subpopulations are typically unique and cell line-specific (Fig. 2C). The main exceptions were seven subpopulations that commonly upregulated cell cycle-related genes, and six subpopulations that commonly upregulated stress response genes. Similar results were obtained using DBSCAN with different parameters (fig. S2C–D).

To also identify continuous variability of cellular states, we applied non-negative matrix factorization (NMF) to each cancer cell line⁵. We repeated the NMF analysis with distinct parameters, to identify robust expression programs (*i.e.* consistently observed as variable using different parameters), each defined by the top 50 genes based on NMF scores (e.g., Fig. 2D; Methods). This procedure captures both continuous and discrete programs. Overall, we detected 1,445 robust expression programs across all cell lines, with 4-9 such programs

in individual cell lines (fig. S2E; Table S3). To identify common expression programs varying within multiple cell lines, we first excluded those with limited similarity to all other programs as well as those associated with the technical confounder of low data quality (fig. S2F), retaining 800 programs (0-8 per cell line, fig. S2E). Of these programs, only 4.75% corresponded to the discrete subpopulations above (Fig. 2E).

Hierarchical clustering of the NMF programs based on their shared genes emphasized multiple recurrent heterogeneous programs (RHPs) of gene expression, which are present in multiple cell lines. As expected, the two most prominent RHPs reflected the cell cycle, and 10 additional RHPs were associated with other cellular processes but were not positively associated with the cell cycle (Fig. 2E; Table S4). The cell cycle RHPs corresponded to the G1/S and the G2/M phases (Fig. 2E), as was also observed in clinical tumor samples (fig. S3A). G2/M programs were highly similar across cell lines, as well as between cell lines and tumors, thus defining a generic mitotic program (fig. S3B). In contrast, G1/S programs differed more both across cell lines and between cell lines and tumors (fig. S3B), indicating that expression programs associated with genome replication are more context-dependent. A central difference in G1/S programs involved the MCM complex genes (MCM2-7) and the linker histone H1 family genes (HIST1H1B-E), which were robustly upregulated only in tumors or cell lines, respectively (fig. S3B,D). This may reflect an *in vitro* adaptation to rapid growth and loss of the G1 checkpoint in cell lines. Consistent with this possibility, while tumors have a high percentage of apparent G0 cells (*i.e.*, lacking both G1/S and G2/M expression programs), such cells are much less prevalent in cell lines (fig. S3E).

RHPs reflect distinct biological processes and mirror *in vivo* states

The ten additional RHPs reflect diverse biological processes, and are each described in detail in the next sections (Fig. 3 and Table S4). These RHPs were either largely independent of cell cycle status or preferentially expressed by non-cycling cells (fig S4A,B). Importantly, each of the RHPs were detected across at least 8 different cell lines and from at least four different pools, highlighting their robustness (fig. S4C). We characterized these 10 RHPs by functional enrichment of their signature genes (Fig. 3D), by the cell lines in which they are observed (fig. S4D,E), and by their potential regulators²³ (Table S5–6).

In addition, we examined the similarity of these *in vitro* RHPs with recurrent *in vivo* expression programs that vary across cells within patient tumor samples. *In vivo* RHPs were defined previously in HNSCC⁵, melanoma⁶, glioblastoma²⁴, and ovarian cancer²⁵, and we defined additional RHPs by NMF analysis of scRNA-seq datasets in HNSCC⁵, melanoma⁶, breast cancer⁹ and lung cancer¹² samples (fig. S3A and Table S7). Strikingly, 7 out of the 10 cell line RHPs are highly similar to the *in vivo* RHPs, as defined by highly significant overlap of signature genes (Fig. 4A, FDR-adjusted $p < 10^{-9}$ by hypergeometric test), as well as by high correlation of cell scores (Fig. 4B). The *in vivo* relevance of cell line RHPs was further demonstrated in melanoma and in HNSCC by a combined analysis of cells from cell lines and tumors, demonstrating their common patterns of variation as described below (Fig. 4C–F and S5).

RHPs are associated with multiple types of stress responses

One of the RHPs (#8) reflected a stress response, including DNA damage-induced and immediate early genes (*e.g.* DDIT3-4 and ATF3). This RHP resembles programs of heterogeneity previously observed in melanoma and HNSCC tumors^{5,6} (Fig. 4A,B), and may reflect the response to various cellular insults. Another RHP (#4) contained interferon (IFN) response genes (*e.g.*, IFT1-3 and ISG15,20), highly resembling a program of heterogeneity observed within ascites samples of ovarian cancer patients²⁵. Recent studies revealed that IFN response may be triggered by genomic instability through the cGAS-STING pathway²⁶. Accordingly, the IFN-response program was depleted in cell lines with mutations in MRE11A (fig. S6A), which recognizes cytosolic dsDNA and activates STING²⁷.

Two other RHPs (#9 and #10) consisted of genes related to protein folding and maturation (*e.g.* HSPA1A, RPN2) and to proteasomal degradation (*e.g.* PSMA3-4), respectively. These RHPs were the only ones that did not seem to resemble any of the *in vivo* programs of heterogeneity observed previously among tumor cells. However, it is possible that such programs exist *in vivo* and have not been detected yet due to the limited scRNA-seq data in tumors.

RHPs recapitulate *in vivo* EMT programs, and are associated with specific cancer types and NOTCH mutations

Three distinct RHPs were related to EMT: two shared across cancer types, and one unique to melanoma cell lines (fig. S4D). The melanoma-specific EMT (RHP #2; EMT-I) was negatively correlated with another melanoma-specific RHP (#1) that was enriched with skin pigmentation genes (*e.g.*, MITF and PMEL). Both of these melanoma-specific RHPs, and their negative correlation, recapitulated the patterns of variability previously observed in melanoma tumors (Fig. 4A,B), in which they were linked to drug resistance^{6,13}. Accordingly, these two RHPs were associated with three of the top five principle components, and with a range of cellular states, in a combined analysis of *in vitro* and *in vivo* melanoma cells (Figs. 4C,E, S5A,B,E). Notably, as observed in patient samples, many of the melanoma cell lines (50%; Table S3) harbored cells in both of these alternate cellular states, yet our data highlight certain melanoma cell lines as more faithful model systems for these *in vivo*-related RHPs (fig. S5E).

Two other RHPs, EMT-II (#3) and EMT-III (#5), also reflected EMT-like processes in distinct cell lines. EMT-II was mainly observed in HNSCC cell lines, although across 7 distinct pools (fig. S4C,D). It included vimentin (VIM), fibronectin (FN1), the AXL receptor tyrosine kinase, and other genes, closely mirroring the partial EMT state we previously observed in HNSCC tumors (Figs. 4A,B,D,F, S5), where it was linked to metastasis⁵. Cell lines harboring EMT-II were depleted of *NOTCH4* mutations (fig. S6A) and were more sensitive to inhibitors of NOTCH signaling (fig. S6B), suggesting a potential role of the NOTCH pathway in enabling EMT-II variability. This is similar to the association we found in glioblastoma between specific mutations and patterns of intra-tumoral heterogeneity²⁴. In contrast, EMT-III was enriched among non-cycling cells (fig. S4A,B) and contained genes

involved in cell junction organization such as laminin A3, B3 and C3, and plakoglobin (JUP). Interestingly, JUP was shown to promote collective migration of circulating tumor cells with increased metastatic potential²⁸. The identification of three distinct EMT programs, two of which are enriched in specific cancer types, highlights EMT as a common, yet context-specific, pattern of cellular heterogeneity, which may have important implications for metastasis and drug responses.

RHPs related to classical and epithelial senescence programs

RHPs #6 and #7 were preferentially observed in G0 cells (fig. S4A,B) and seem to reflect different expression programs related to cellular senescence. RHP #6 was enriched in p53-wild type cell lines and in those sensitive to the pharmacological activation of p53 by the MDM2 inhibitor Nutlin-3a (fig. S6). Moreover, it included the senescence mediator p21 (CDKN1A) and other p53-target genes. Thus, we annotated it as “classical” p53-dependent senescence. In contrast, RHP #7 was not enriched in p53-wild type cell lines, but was enriched in HNSCC cell lines (fig. S4D,E).

RHP #7 was highly similar to the senescence program of keratinocytes and had similarity to other published senescence programs^{29–32} (Figs. 5A, S7A,B, Table S8). To further examine the similarity of RHP #7 with senescence-related programs of epithelial cells, we profiled primary lung bronchial cells by bulk RNA-seq after induction of senescence by etoposide. The etoposide-treated cells stained for the senescence marker SA- β -GAL and strongly downregulated the expression of cell cycle genes, indicating a bona fide senescence phenotype (Fig. 5B). Both of the senescence-associated RHPs (#6 and #7) were upregulated, although the effect was stronger for RHP #7 genes, which were among the top upregulated genes (Fig. 5B, S7C). RHP #7 also contained many secreted factors, consistent with a Senescence-Associated Secretory Phenotype (SASP). These include S100A8, S100A9, SAA1, SAA2, LCN2, CXCL1 and SLPI, which are involved in inflammatory responses and may influence cancer, stromal and immune cells in the tumor microenvironment. While most of these factors are not traditionally considered as classical SASP genes³³, we found a significant overlap ($P < 0.01$, hypergeometric test) with secreted factors from multiple other senescence-related programs, including from the *in vivo* counterpart in HNSCC tumors (fig. S7D,E).

Taken together, RHP #7 is associated with low proliferation and a secretory phenotype, and highly resembles the senescence response of keratinocytes, lung bronchial cells, and other epithelial cells. It lacks classical senescence markers (*e.g.*, p16 and p21) and differs from published senescence signatures of fibroblasts and melanocytes²⁹, underscoring the context-specificity of senescence expression programs. We therefore denote it as an epithelial senescence-associated (EpiSen) program. We note that although the EpiSen program is induced in senescent cells, its expression does not necessarily imply a complete senescent phenotype.

Notably, EpiSen recapitulates a program we previously observed in HNSCC tumors, “Epi-Difl” (Figs. 4A,B, 5A), which was negatively associated with the cell cycle and spatially restricted to the hypoxic tumor core⁵. This program was negatively correlated with the EMT-

II program, defining a spectrum of cellular states that is shared by multiple HNSCC cell lines and tumors. Accordingly, the two RHPs were associated with three of the top five principle components, and with a range of cellular states, in a combined analysis of *in vitro* and *in vivo* HNSCC cells (Fig. 4D,F, S5C–E).

Proliferation and dynamics of EpiSen subpopulations in HNSCC

We selected two HNSCC cell lines (JHU006 and SCC47) with high variability of the EpiSen and EMT-II RHPs for further analysis. EpiSen-high and EpiSen-low subpopulations of cells could be prospectively isolated by FACS (as AXL⁻/CLDN4⁺ and AXL⁺/CLDN4⁻, respectively, fig. S8A), with ~12-fold difference in the expression of the EpiSen program (Fig. 5C). We note that EpiSen-low cells are only minimally enriched for the EMT-II RHP, and are used here as a negative control for the EpiSen RHP. The EpiSen-high subpopulation was enriched for G0/G1 phases, consistent with lower proliferation (Fig. 5D, S8B). Nevertheless, it still contained cells in the S and G2/M phases, similar to its *in vivo* counterpart (fig. S8C) and did not stain for the classical senescence marker SA-β-gal (data not shown). These results suggest that the EpiSen program represent an incomplete or reversible cell cycle arrest, consistent with previous studies in cancer cells³⁴.

Interestingly, the EpiSen-high and EpiSen-low sorted subpopulations began to shift by one week in culture and each of them returned to the pre-sorting distribution of cellular states by four weeks, suggesting cellular transitions (Figs. 5E, S8D). This distribution of cellular states was stably maintained in culture, suggesting a steady-state which is maintained through a balance between proliferation (favoring EpiSen-low cells) and cellular transitions (favoring EpiSen-high cells). These results indicate that the EpiSen program is dynamically regulated, although we cannot determine if cellular transitions occur only from EpiSen-low to EpiSen-high or in both directions.

RHP regulation by genetics and tumor microenvironment

Expression heterogeneity could be driven by either genetic or non-genetic mechanisms. To search for the contribution of genetic heterogeneity, we identified large-scale copy number aberrations (CNAs) in each cell, based on average expression levels in windows of 100 genes around each locus^{3–8} (fig. S9). CNA patterns allowed the robust identification of multiple genetic subclones in 26% (58/198) of the cell lines, based on the gain or loss of chromosomes (or chromosome arms) that was restricted to subsets of cells (Methods). Co-existence of genetic subclones is consistent with ongoing evolutionary dynamics within cell lines, as demonstrated recently¹⁵. Next, we compared the assignment of cells to CNA-based genetic subclones with their patterns of expression heterogeneity. Among the discrete expression-based clusters, 39% were significantly associated with specific genetic subclones, suggesting a genetic basis for these cases of expression heterogeneity (Fig. 6A–B; $P < 0.001$, Fisher's exact test). In contrast, only 8% of the continuous NMF programs were significantly associated with genetic subclones (Fig. 6B, $P < 0.001$, t-test). This analysis likely underestimates the contribution of genetic heterogeneity, as it relies on CNAs for subclone identification. However, it suggests that genetic heterogeneity contributes primarily to discrete clusters, while the continuous programs of heterogeneity may primarily reflect

cellular plasticity, consistent with the established plasticity of EMT and the dynamics of the EpiSen program described above.

Next, we examined the induction of these programs by soluble factors that are secreted by components of the tumor microenvironment and by related perturbations. The most dynamic programs were EMT-II and EpiSen, which responded in opposite ways to several of the perturbations (Fig. 6C, fig. S10A). As expected, TGF- β 1 and TGF- β 3 upregulated the expression of the EMT-II genes and increased migration in a wound healing assay (fig. S10B–C). Interestingly, TGF- β treatments also downregulated the expression of EpiSen genes, underscoring the potential interplay between EpiSen and EMT. A negative association between these two programs was further supported by the single cell profiles of HNSCC cell lines and tumors (Fig. 4D,F, S5E) and by our prior findings that EMT-high cells were enriched at the invasive edge, while EpiSen-high cells were enriched at the core of tumors⁵. Tumor cores are often associated with increased hypoxia, suggesting a potential mechanism for the spatial enrichment of senescent cells. In accordance with this possibility, the hypoxia mimetic desferrioxamine (DFO) induced the expression of the EpiSen program. A similar effect was observed upon hydrogen peroxide treatment, consistent with oxidative stress as a potent inducer of senescence³⁵ (Fig. 6C). Taken together, the EpiSen and EMT-II programs reflect cellular plasticity that exists in certain cell lines even in the absence of perturbations and the native tumor microenvironment, but they are further induced by stresses (e.g. hypoxia and oxidative stress) and by secreted factors (e.g. TGF- β).

Co-existing subpopulations differ in drug sensitivity

An important implication of cellular diversity in cancer is the possibility that distinct subpopulations of cells respond differently to treatments and thereby facilitate treatment failure and recurrence. Thus, we compared the sensitivities of EpiSen-high and EpiSen-low subpopulations sorted from each of the two model cell lines selected (Fig. 7A). We initially screened 2,198 bioactive compounds using a CTG-based viability assay (fig. S11A–C). Putative hits ($n=248$) defined based on differential sensitivity or the ability to kill both subpopulations ($<10\%$ viability) were selected for a secondary screen performed in duplicates in each cell line (Fig. 7B). Compounds that killed both subpopulations in the primary screen were tested at reduced concentration in the secondary screen. The secondary screen identified 113 compounds with differential killing of the subpopulations in at least one cell line (Table S9).

Of the hits with preferential sensitivity of EpiSen-high cells, $>40\%$ were shared between both cell lines. This fraction of shared hits further increases to 71.4% (for both cell lines) when considering the targets of compounds rather than the exact compounds, highlighting consistent vulnerabilities of EpiSen-high cells. Fourteen compounds with differential sensitivities, including five shared hits and nine that were specific to one cell line, were analyzed by a full dose response (Figs. 7C, S11D, Table S10). All five of the shared compounds, and five of the nine cell line-specific compounds (56%), displayed significant differential sensitivity as in the secondary screen ($P<0.05$, paired t-test).

As expected, EpiSen-high cells were more sensitive to the senolytic compound ABT-737³⁶ while EpiSen-low cells were preferentially sensitive to inhibitors of cell cycle regulators (CDKs, CHK1 and topoisomerase), consistent with their increased proliferation. Additional EpiSen-high sensitivities included multiple inhibitors of EGFR, AKT, PI3K, DNA-PK, IGF1R, and JAK (Fig. 7B). Several of these targets (DNA-PK, IGF1R and AKT) converge on repair of double-strand breaks as part of the DNA repair machinery^{37,38}. Together with the observation that hydrogen peroxide induces the expression of EpiSen genes (Fig. 6C), these results reinforce the role of DNA damage as a potential inducer of this RHP. The PI3K/AKT axis is hyper-activated in HNSCC, and resistance to PI3K inhibition in HNSCC is AXL-dependent³⁹. Accordingly, EpiSen-high cells (which are defined by low AXL expression) were more sensitive to inhibitors of PI3K and AKT, as well as those of EGFR and IGF1R that signal via the PI3K/AKT axis.

Apart from cell cycle inhibitors, EpiSen-low cells in SCC47 (HPV+, p53 WT) also had increased sensitivity to multiple proteasome inhibitors. In contrast, all subpopulations of JHU006 (HPV-) were sensitive to proteasomal inhibition. The differential sensitivity to proteasomal inhibitors between different HNSCC cell lines is consistent with previous studies, which ascribed those differences to HPV and p53 status⁴⁰ and to activation of NFkB⁴¹. Our analysis further highlights differential sensitivity to such inhibitors within the same cell line (SCC47) and a connection to the EpiSen program. EpiSen-low cells in SCC47 also had increased sensitivity to drugs that induce cell death by sensitizing cells to ferroptosis (the GPX4 inhibitor RSL3, Erastin, and the SLC7A11 inhibitor Sorafenib) (Fig. 7B). Recent work demonstrated that mesenchymal cells are particularly sensitive to ferroptosis-inducing compounds^{42,43}. Thus, sensitivity to ferroptosis-inducing compounds may be increased in cells with mesenchymal features, consistent with previous work, and decreased in cells with features of senescence.

Taken together, EpiSen-high and EpiSen-low cells are associated with differential vulnerabilities that are largely consistent across two model cell lines and potentially across human tumors. In addition to these differential sensitivities, we also observed consistent sensitivities between EpiSen-high and EpiSen-low cells that were shared between cell lines. Nine compounds killed both subpopulations (viability < 10%) in both of the cell lines (Table S9), including disulfiram (Antabuse), which was proposed recently as a potential HNSCC therapy^{44,45}.

EpiSen subpopulations are predictive of clinical drug response

Of the multiple differential vulnerabilities described above, the increased sensitivity of EpiSen-high cells to multiple EGFR inhibitors captured our interest due to its potential clinical relevance. Cetuximab is an EGFR inhibitor routinely used for the treatment of HNSCC patients⁴⁶. Most patients with recurrent or metastatic HNSCC progress shortly after Cetuximab treatment, combined with platinum-based chemotherapy, but a minority of patients have long progression-free survival (PFS). To examine the potential relevance of EpiSen in clinical response to Cetuximab, we examined bulk pre-treatment transcriptome data of 40 recurrent or metastatic HNSCC patients, stratified by PFS following Cetuximab

treatment⁴⁶. Twenty six patients had short PFS (PFS<5.6 months) while fourteen patients had long PFS (PFS>12 months).

Consistent with our *in vitro* observations, patients with long PFS had significantly higher EpiSen scores compared to those with short PFS (Fig. 7D–E, fig. S12). Accordingly, bulk EpiSen scores, a proxy for the abundance of EpiSen cells, were predictive of patients' responses, with an area under curve (AUC) of 0.86. For example, a potential EpiSen threshold identifies 79% (11/14) of the long PFS but only 23% (6/26) of the short PFS patients, corresponding to sensitivity of 79% and specificity of 77%. While this predictive power may not be sufficient for clinical use, future work and larger cohorts may consider a combination of EpiSen with other features for improved prediction. Notably, the predictive power of EpiSen was comparable between the HNSCC *in vitro* RHP defined in this work and the *in vivo* program defined previously, and was slightly higher for the shared genes among the two programs (Fig. 7E).

Discussion

Our analysis of cell lines identified 12 RHPs (2 cell cycle and 10 others), 9 of which were highly similar to programs of heterogeneity observed within tumors, indicating that they are retained in the absence of a native microenvironment. The continuous pattern of such RHPs contrasts with the discrete nature of genetic heterogeneity. Accordingly, we observed dynamic plasticity of the EpiSen program and found only limited associations with genetic subclones (albeit only by inferred CNAs). Thus, cancer cells may harbor variability through two largely distinct processes of genetic and nongenetic mechanisms, both of which may contribute to drug resistance and tumor progression. We speculate that by focusing on recurrent patterns of heterogeneity our analysis highlights nongenetic plasticity, as this form of variability tends to be shared across cell lines, while genetic forms of variability may be more unique to each cell line.

We suggest that the significance of RHPs is derived directly from their definition as recurrent. A central observation from scRNA-seq studies of tumors is that although each tumor is unique, the diversity of cancer cells *within* individual tumors highlights few programs that recur as heterogeneous across many tumors⁴⁷. Here we show that some of these programs also recur as heterogeneous in specific cell lines, sometimes across multiple cancer types, paving the way for mechanistic and functional studies. Just as cancer genetics has focused on recurrent mutations, based on the premise that they are drivers of tumorigenesis, we propose that cancer transcriptomics should focus on recurrent programs, as they may drive important cancer phenotypes, such as drug resistance and metastasis. Extending the analogy to therapeutics, we envisage that while current targeted therapies attempt to reverse the action of recurrent oncogenic mutations, future targeted therapies may also be targeted at recurrent programs associated with proliferation, drug resistance or metastasis.

Careful examination of the recurrent *in vitro* programs highlights their consistency with *in vivo* tumor programs, but also the divergence from their developmental “normal” counterparts. During development and wound healing, both EMT and senescence are

associated with precise phenotypes and well-defined regulators. Yet in the context of tumors and cancer cell lines, we observe only partial phenotypes and limited dependence on these regulators. The EMT-like profiles we observe include many EMT-related genes and are associated with increased migration, but do not involve other EMT hallmarks such as the loss of epithelial markers, a drastic change in morphology, and high expression of EMT transcription factors. Similarly, EpiSen-high cells resemble the senescence response of keratinocytes and lung bronchial cells, are associated with reduced proliferation, and possess markers of SASP, yet they retain some proliferative capacity, do not express high levels of p16 and p21, and do not stain with SA- β -GAL. This is consistent with studies showing evidence for incomplete and reversible senescence programs in cancer: Low levels of p16 at induction of senescence may confer cell cycle re-entry upon p53 inactivation or RAS expression⁴⁸, a program coined “light senescence”³⁴ and likewise, loss of Rb in senescent cells may lead to renewed proliferation⁴⁹. We hypothesize that cancer cells often activate partial or distorted programs, possibly not through the canonical developmental mechanisms, and in a context-dependent manner. This could contribute to the difficulties in resolving long-standing debates in the cancer field about the role of EMT and senescence, which are often evaluated through the activity of developmental regulators and markers that may fail to detect certain partial programs. Comprehensive single cell profiling helps to detect such partial programs that vary in their magnitude across the cells.

Multiple RHPs are of potential clinical relevance. First, the EpiSen program, which mirrors subpopulations of cells detected in HNSCC tumors, is associated with distinct responses to several drugs. Notably, the sensitivity of EpiSen-high cells to EGFR inhibitors appears to extend from cell lines to patients, underscoring its significance. These results provide a rationale for the combination of EpiSen-killing drugs (e.g. Cetuximab) with chemotherapies that target the more proliferative subpopulations. Second, for two EMT-like RHPs (EMT-I and EMT-II), clinical relevance is strongly supported by previous studies of tumor samples. EMT-II is highly consistent with a heterogeneity program we previously described in HNSCC tumors⁵, where it was shown to be localized to the invasive edge of the tumor and predictive of nodal metastasis. Recent work further evaluated the quantification of this program as a tool for clinical decision making⁵⁰.

Similarly, EMT-I, seen only in melanoma cell lines, is highly consistent with a heterogeneity program we previously described in melanoma tumors⁶. Moreover, other studies defined different versions of this program, both in tumors and in cell lines, variably naming it as an ‘invasive’^{51,52}, ‘AXL-high’/‘MITF-low’^{53,54}, or ‘resistance’¹³ program, but invariably involving upregulation of EMT-related genes, downregulation of skin pigmentation genes (e.g. MITF) and resistance to targeted therapies. While the specific definition of this program varies between studies, this overall convergence indicates a robust phenomenon in melanoma whereby tumors often consist of drug-sensitive and drug-resistant subpopulations that differ in levels of pigmentation and EMT-related genes, which are recapitulated here by the Skin pigmentation and EMT-I RHPs.

For two other RHPs, our observations in cell lines suggest a potential for clinical relevance, although further studies would be needed to evaluate this. The p53-dependent senescence program (RHP #6) is significantly correlated with response to the p53 activating drug,

Nutlin-3a. Notably, in Nutlin-sensitive cell lines, only a minority of cells express this program before treatment, while most or all cells appear to express it after treatment⁵⁵, suggesting that rare senescent cells may serve as a biomarker for p53 activity that implies sensitivity to Nutlin-3a or similar treatments. Although p53 mutations are routinely tested, the multitude of functionally distinct p53 mutations and of other mechanisms that influence p53 activity warrant a direct functional readout in case p53-based treatments will be incorporated in clinical practice. Third, expression of the IFN response program (RHP #4) by subpopulations of cancer cells, as recently described in ovarian cancer²⁵, may influence immune cells in the tumor microenvironment and the response to immunotherapies. For example, recent work demonstrated opposing functions of the IFN response by cancer and immune cells through complex cancer-immune crosstalk⁵⁶.

With the advent of single cell genomics, cellular heterogeneity is now being characterized in various clinical contexts. However, the ability to model ITH is a prerequisite for deeper understanding of the mechanisms that govern such heterogeneity. Here we described the landscape of cellular diversity across ~200 cell lines, highlighting particular models that recapitulate programs of heterogeneity observed in human tumors. Further studies of these programs and model systems will provide a better understanding of ITH, and may help to transform this understanding to novel treatment strategies that exploit ITH.

Supplementary Material

Refer to Web version on PubMed Central for supplementary material.

Acknowledgements

This work was supported by funding from the Israel Science Foundation (I.T.), the Zuckerman STEM leadership program (I.T.), the Mexican Friends New Generation grant (I.T.), the Rising Tide Foundation (I.T.), the A.M.N. Fund for the Promotion of Science, Culture and Arts in Israel (I.T.), the Estate of Dr. David Levinson, the Dr. Celia Zwillenberg-Fridman and Dr. Lutz Zwillenberg Career Development Chair (I.T.), the Sao Paulo Research Foundation (FAPESP) Fellowship 2014/27287-0 and 2017/24287-8 (G.S.K.), the Clore Foundation Postdoctoral Fellowship (A.C.G.), the Klarman Cell Observatory (A.R.) and HHMI (A.R.).

Data availability

Raw and processed scRNA-seq data is available through the Broad Institute's single cell portal (SCP542).

References

1. McGranahan N & Swanton C Biological and therapeutic impact of intratumor heterogeneity in cancer evolution. *Cancer Cell* 27, 15–26 (2015). [PubMed: 25584892]
2. Chaffer CL, San Juan BP, Lim E & Weinberg RA EMT, cell plasticity and metastasis. *Cancer Metastasis Rev* 35, 645–654 (2016). [PubMed: 27878502]
3. Filbin MG et al. Developmental and oncogenic programs in H3K27M gliomas dissected by single-cell RNA-seq. *Science* 360, 331–335 (2018). [PubMed: 29674595]
4. Patel AP et al. Single-cell RNA-seq highlights intratumoral heterogeneity in primary glioblastoma. *Science* 344, 1396–401 (2014). [PubMed: 24925914]
5. Puram S et al. Single-cell transcriptomic analysis of primary and metastatic tumor ecosystems in head and neck cancer. *Cell* (2017).

6. Tirosh I et al. Dissecting the multicellular ecosystem of metastatic melanoma by single-cell RNA-seq. *Science* 352, 189–96 (2016). [PubMed: 27124452]
7. Tirosh I et al. Single-cell RNA-seq supports a developmental hierarchy in human oligodendroglioma. *Nature* 539, 309–313 (2016). [PubMed: 27806376]
8. Venteicher AS et al. Decoupling genetics, lineages, and microenvironment in IDH-mutant gliomas by single-cell RNA-seq. *Science* 355(2017).
9. Chung W et al. Single-cell RNA-seq enables comprehensive tumour and immune cell profiling in primary breast cancer. *Nat Commun* 8, 15081 (2017). [PubMed: 28474673]
10. Kim KT et al. Application of single-cell RNA sequencing in optimizing a combinatorial therapeutic strategy in metastatic renal cell carcinoma. *Genome Biol* 17, 80 (2016). [PubMed: 27139883]
11. Li H et al. Reference component analysis of single-cell transcriptomes elucidates cellular heterogeneity in human colorectal tumors. *Nat Genet* 49, 708–718 (2017). [PubMed: 28319088]
12. Lambrechts D et al. Phenotype molding of stromal cells in the lung tumor microenvironment. *Nat Med* 24, 1277–1289 (2018). [PubMed: 29988129]
13. Shaffer SM et al. Rare cell variability and drug-induced reprogramming as a mode of cancer drug resistance. *Nature* 546, 431–435 (2017). [PubMed: 28607484]
14. Jerby-Arnon L et al. A Cancer Cell Program Promotes T Cell Exclusion and Resistance to Checkpoint Blockade. *Cell* 175, 984–997 e24 (2018). [PubMed: 30388455]
15. Ben-David U et al. Genetic and transcriptional evolution alters cancer cell line drug response. *Nature* 560, 325–330 (2018). [PubMed: 30089904]
16. Fillmore CM & Kuperwasser C Human breast cancer cell lines contain stem-like cells that self-renew, give rise to phenotypically diverse progeny and survive chemotherapy. *Breast Cancer Res* 10, R25 (2008). [PubMed: 18366788]
17. Gupta PB et al. Stochastic state transitions give rise to phenotypic equilibrium in populations of cancer cells. *Cell* 146, 633–44 (2011). [PubMed: 21854987]
18. Stackpole CW Generation of phenotypic diversity in the B16 mouse melanoma relative to spontaneous metastasis. *Cancer Res* 43, 3057–65 (1983). [PubMed: 6850615]
19. Barretina J et al. The Cancer Cell Line Encyclopedia enables predictive modelling of anticancer drug sensitivity. *Nature* 483, 603–7 (2012). [PubMed: 22460905]
20. Ghandi M et al. Next-generation characterization of the Cancer Cell Line Encyclopedia. *Nature* 569, 503–508 (2019). [PubMed: 31068700]
21. Yu C et al. High-throughput identification of genotype-specific cancer vulnerabilities in mixtures of barcoded tumor cell lines. *Nat Biotechnol* 34, 419–23 (2016). [PubMed: 26928769]
22. Kang HM et al. Multiplexed droplet single-cell RNA-sequencing using natural genetic variation. *Nat Biotechnol* 36, 89–94 (2018). [PubMed: 29227470]
23. Aibar S et al. SCENIC: single-cell regulatory network inference and clustering. *Nat Methods* 14, 1083–1086 (2017). [PubMed: 28991892]
24. Neftel C et al. An Integrative Model of Cellular States, Plasticity, and Genetics for Glioblastoma. *Cell* 178, 835–849 e21 (2019). [PubMed: 31327527]
25. Izar B et al. A single-cell landscape of high-grade serous ovarian cancer. *Nature Medicine* (2020).
26. Chen Q, Sun L & Chen ZJ Regulation and function of the cGAS-STING pathway of cytosolic DNA sensing. *Nat Immunol* 17, 1142–9 (2016). [PubMed: 27648547]
27. Kondo T et al. DNA damage sensor MRE11 recognizes cytosolic double-stranded DNA and induces type I interferon by regulating STING trafficking. *Proc Natl Acad Sci U S A* 110, 2969–74 (2013). [PubMed: 23388631]
28. Aceto N et al. Circulating tumor cell clusters are oligoclonal precursors of breast cancer metastasis. *Cell* 158, 1110–1122 (2014). [PubMed: 25171411]
29. Hernandez-Segura A et al. Unmasking Transcriptional Heterogeneity in Senescent Cells. *Curr Biol* 27, 2652–2660 e4 (2017). [PubMed: 28844647]
30. Jang DH et al. A transcriptional roadmap to the senescence and differentiation of human oral keratinocytes. *J Gerontol A Biol Sci Med Sci* 70, 20–32 (2015). [PubMed: 24398559]

31. Musiani D et al. PRMT1 Is Recruited via DNA-PK to Chromatin Where It Sustains the Senescence-Associated Secretory Phenotype in Response to Cisplatin. *Cell Rep* 30, 1208–1222 e9 (2020). [PubMed: 31995759]
32. Yang L, Fang J & Chen J Tumor cell senescence response produces aggressive variants. *Cell Death Discov* 3, 17049 (2017). [PubMed: 28845296]
33. Coppe JP, Desprez PY, Krtolica A & Campisi J The senescence-associated secretory phenotype: the dark side of tumor suppression. *Annu Rev Pathol* 5, 99–118 (2010). [PubMed: 20078217]
34. Lee S & Schmitt CA The dynamic nature of senescence in cancer. *Nat Cell Biol* 21, 94–101 (2019). [PubMed: 30602768]
35. te Poele RH, Okorokov AL, Jardine L, Cummings J & Joel SP DNA damage is able to induce senescence in tumor cells in vitro and in vivo. *Cancer Res* 62, 1876–83 (2002). [PubMed: 11912168]
36. Yosef R et al. Directed elimination of senescent cells by inhibition of BCL-W and BCL-XL. *Nat Commun* 7, 11190 (2016). [PubMed: 27048913]
37. Bozulic L, Surucu B, Hynx D & Hemmings BA PKBalpha/Aktl acts downstream of DNA-PK in the DNA double-strand break response and promotes survival. *Mol Cell* 30, 203–13 (2008). [PubMed: 18439899]
38. Wong RH et al. A role of DNA-PK for the metabolic gene regulation in response to insulin. *Cell* 136, 1056–72 (2009). [PubMed: 19303849]
39. Elkabets M et al. AXL mediates resistance to PI3Kalpha inhibition by activating the EGFR/PKC/mTOR axis in head and neck and esophageal squamous cell carcinomas. *Cancer Cell* 27, 533–46 (2015). [PubMed: 25873175]
40. Li C & Johnson DE Liberation of functional p53 by proteasome inhibition in human papilloma virus-positive head and neck squamous cell carcinoma cells promotes apoptosis and cell cycle arrest. *Cell Cycle* 12, 923–34 (2013). [PubMed: 23421999]
41. Chen Z et al. Differential bortezomib sensitivity in head and neck cancer lines corresponds to proteasome, nuclear factor-kappaB and activator protein-1 related mechanisms. *Mol Cancer Ther* 7, 1949–60 (2008). [PubMed: 18645005]
42. Hangauer MJ et al. Drug-tolerant persister cancer cells are vulnerable to GPX4 inhibition. *Nature* 551, 247–250 (2017). [PubMed: 29088702]
43. Viswanathan VS et al. Dependency of a therapy-resistant state of cancer cells on a lipid peroxidase pathway. *Nature* 547, 453–457 (2017). [PubMed: 28678785]
44. Park YM et al. Anti-cancer effects of disulfiram in head and neck squamous cell carcinoma via autophagic cell death. *PLoS One* 13, e0203069 (2018). [PubMed: 30212479]
45. Shah O'Brien P et al. Disulfiram (Antabuse) Activates ROS-Dependent ER Stress and Apoptosis in Oral Cavity Squamous Cell Carcinoma. *J Clin Med* 8(2019).
46. Bossi P et al. Functional Genomics Uncover the Biology behind the Responsiveness of Head and Neck Squamous Cell Cancer Patients to Cetuximab. *Clin Cancer Res* 22, 3961–70 (2016). [PubMed: 26920888]
47. Suva ML & Tirosh I Single-Cell RNA Sequencing in Cancer: Lessons Learned and Emerging Challenges. *Mol Cell* 75, 7–12 (2019). [PubMed: 31299208]
48. Beausejour CM et al. Reversal of human cellular senescence: roles of the p53 and p16 pathways. *EMBO J* 22, 4212–22 (2003). [PubMed: 12912919]
49. Sage J, Miller AL, Perez-Mancera PA, Wysocki JM & Jacks T Acute mutation of retinoblastoma gene function is sufficient for cell cycle re-entry. *Nature* 424, 223–8 (2003). [PubMed: 12853964]
50. Parikh AS et al. Immunohistochemical quantification of partial-EMT in oral cavity squamous cell carcinoma primary tumors is associated with nodal metastasis. *Oral Oncol* 99, 104458 (2019). [PubMed: 31704557]
51. Hoek KS et al. Metastatic potential of melanomas defined by specific gene expression profiles with no BRAF signature. *Pigment Cell Res* 19, 290–302 (2006). [PubMed: 16827748]
52. Verfaillie A et al. Decoding the regulatory landscape of melanoma reveals TEADS as regulators of the invasive cell state. *Nat Commun* 6, 6683 (2015). [PubMed: 25865119]

53. Konieczkowski DJ et al. A melanoma cell state distinction influences sensitivity to MAPK pathway inhibitors. *Cancer Discov* 4, 816–27 (2014). [PubMed: 24771846]
54. Muller J et al. Low MITF/AXL ratio predicts early resistance to multiple targeted drugs in melanoma. *Nat Commun* 5, 5712 (2014). [PubMed: 25502142]
55. McFarland JM et al. Multiplexed single-cell profiling of post-perturbation transcriptional responses to define cancer vulnerabilities and therapeutic mechanism of action. *bioRxiv*, 868752 (2019).
56. Benci JL et al. Opposing Functions of Interferon Coordinate Adaptive and Innate Immune Responses to Cancer Immune Checkpoint Blockade. *Cell* 178, 933–948 e14 (2019). [PubMed: 31398344]

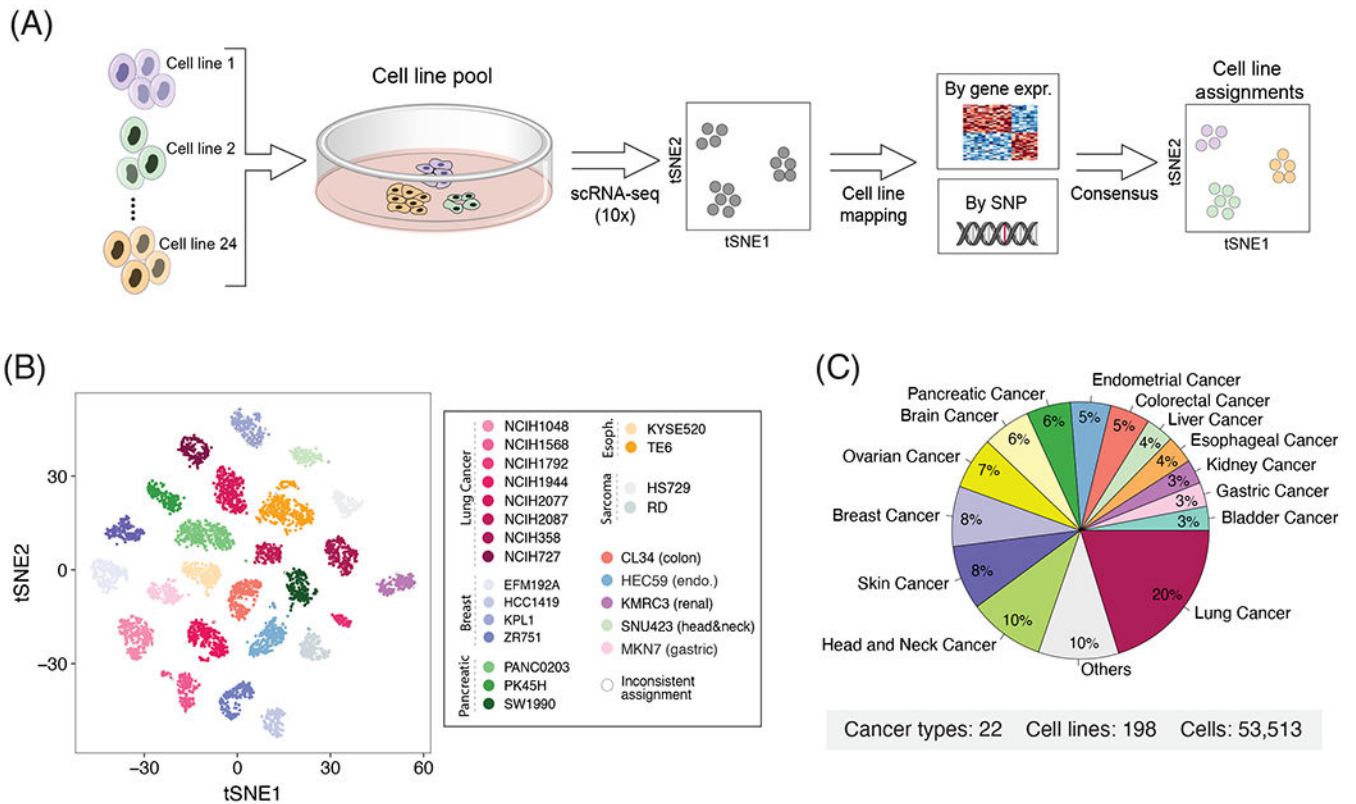


Figure 1. Characterizing intra-cell line expression heterogeneity by multiplexed scRNA-seq.

(A) Workflow of the multiplexing strategy used to profile multiple cell lines simultaneously. Cell lines were pooled and profiled by droplet-based scRNA-seq. We used reference CCLE data to assign cells to the most similar cell line based on their overall gene expression and SNP pattern. (B) t-SNE plot of a representative pool demonstrating the robustness of cells' assignments to cell lines. Cells with inconsistent assignments (by gene expression and SNPs) are denoted and these were excluded from further analyses. (C) Distribution of cancer types profiled.

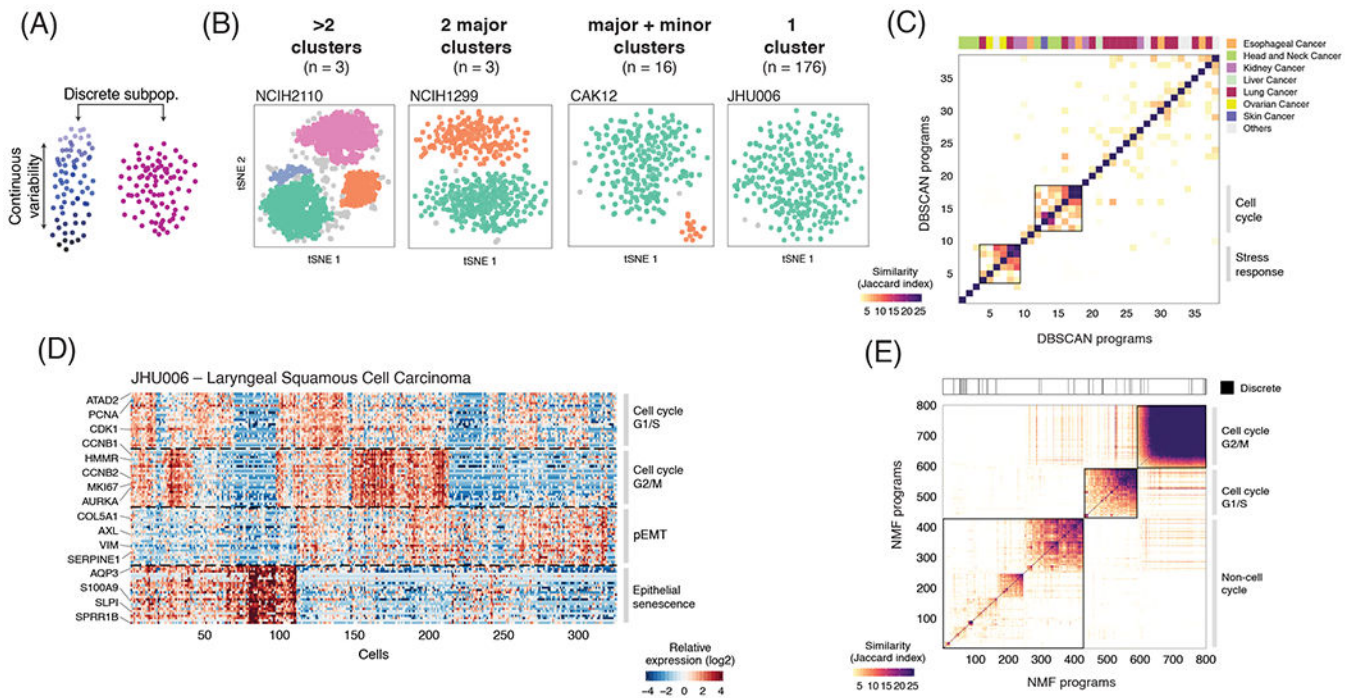


Figure 2. Discrete and continuous patterns of heterogeneity within cell lines.

(A) Illustration of the two types of expression variability investigated. **(B)** t-SNE plots show exemplary cell lines for the four classes defined by the presence and number of discrete subpopulations identified using DBSCAN. The description of each class and number of cell lines is indicated above the t-SNE plots. **(C)** Heatmap depicts pairwise similarities between gene expression programs defined for each of the cell clusters derived from the 22 cell lines identified as having one or more discrete subpopulations. Hierarchical clustering identifies only two groups of similar programs (metaprograms). Top panel shows assignment to cancer types. **(D)** Continuous programs of heterogeneity identified using NMF in a representative cell line that lacks discrete subpopulations (JHU006; see **B**). Heatmap shows relative expression of genes from four programs, across all cells ordered by hierarchical clustering. NMF programs are annotated (right) and selected genes are indicated (left). **(E)** Pairwise similarities between NMF programs identified across all the cell lines analyzed and ordered by hierarchical clustering. Programs with limited similarity to all other programs as well as those associated with technical confounders were excluded. Top panel indicates the 4% of NMF programs that were consistent with discrete subpopulations identified by DBSCAN ($P < 0.001$, Fisher's exact test).

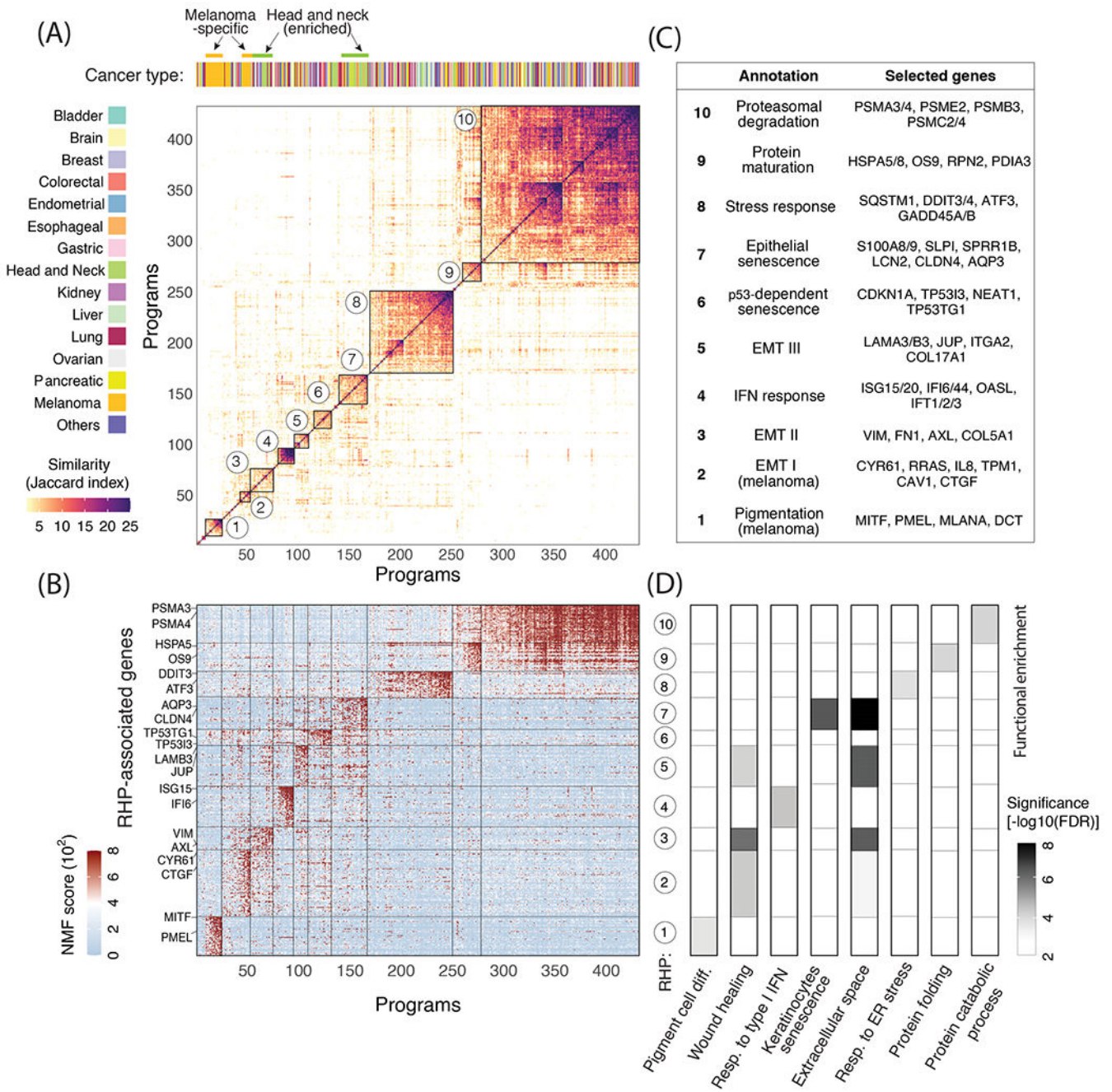


Figure 3. Functional annotation of RHPs.

(A) The main heatmap depicts pairwise similarities between all NMF programs (except for those linked to the cell cycle, see Fig. 2E), ordered by hierarchical clustering. Ten clusters (RHPs) are indicated by squares and numbers. Top panel shows assignment to cancer types, highlighting significant enrichment ($P < 0.05$, hypergeometric test) of melanoma and HNSCC cell lines. (B) NMF scores of signature genes of each RHP (rows), with selected genes labeled. Cells (columns) are ordered as in (A). (C) Annotation and selected top genes for each of the 10 RHPs. (D) Functional enrichment ($-\log_{10}$ of FDR-adjusted p-value, hypergeometric test) of RHP genes with eight annotated gene-sets.

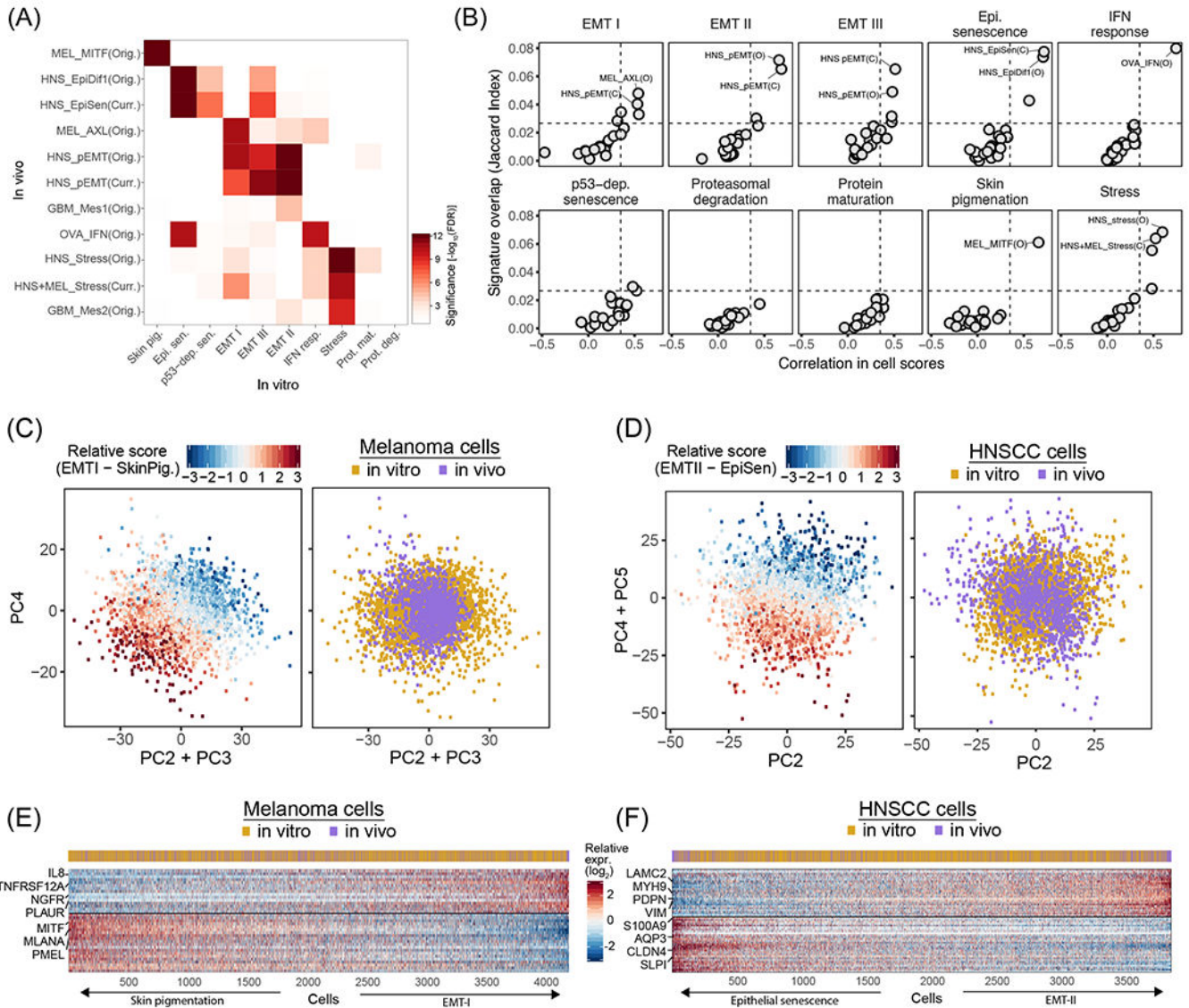


Figure 4. *In vitro* RHPs recapitulate *in vivo* programs of heterogeneity.

(A) Significance of the overlap ($-\log_{10}(P)$ for FDR-adjusted hypergeometric test), between RHP gene-sets defined in cell lines (*in vitro*, X-axis) and in tumors (*in vivo*, Y-axis). *In vivo* RHPs are named by a cancer type abbreviation (MEL: melanoma, HNS: HNSCC, GBM: glioblastoma, OVA: ovarian cancer), followed by an associated functional annotation, and whether it was defined by the original study (Orig.) or the current study (Curr., see Fig. S3).

(B) Each panel shows the mean Jaccard index (Y-axis) and mean correlation of single cell scores (X-axis) between the NMF programs constituting a specific *In vitro* RHP (as noted at the top) and all *In vivo* RHPs. The most similar *In vivo* RHPs are labeled as in (A). Dashed lines indicate a 99.9% confidence threshold determined by permutations of NMF programs.

(C) Scatterplots of melanoma cells based on PC2+PC3 (X-axis) and PC4 (Y-axis). Cells are colored by the relative score for EMT-I and SkinPig genes shared between cell lines and tumors RHPs (left panel) and by whether the cells are from tumors or cell lines (right panel).

(D) Scatterplots of HNSCC cells based on PC2 (X-axis) and PC4+PC5 (Y-axis). Cells are

colored by the relative score for EMT-II and EpiSen genes shared between cell lines and tumors RHPs (left panel) and by whether the cells are from tumors or cell lines (right panel). **(E)** Heatmap showing the relative expression of shared EMT-I and SkinPig RHP genes (rows) across melanoma cells (columns), sorted by the relative RHP scores. The cells' origin from tumors or cell lines is shown by the top panel. **(F)** Heatmap showing the relative expression of shared EMT-II and EpiSen RHP genes (rows) across HNSCC cells (columns), sorted by the relative RHP scores. The cells' origin from tumors or cell lines is shown by the top panel.

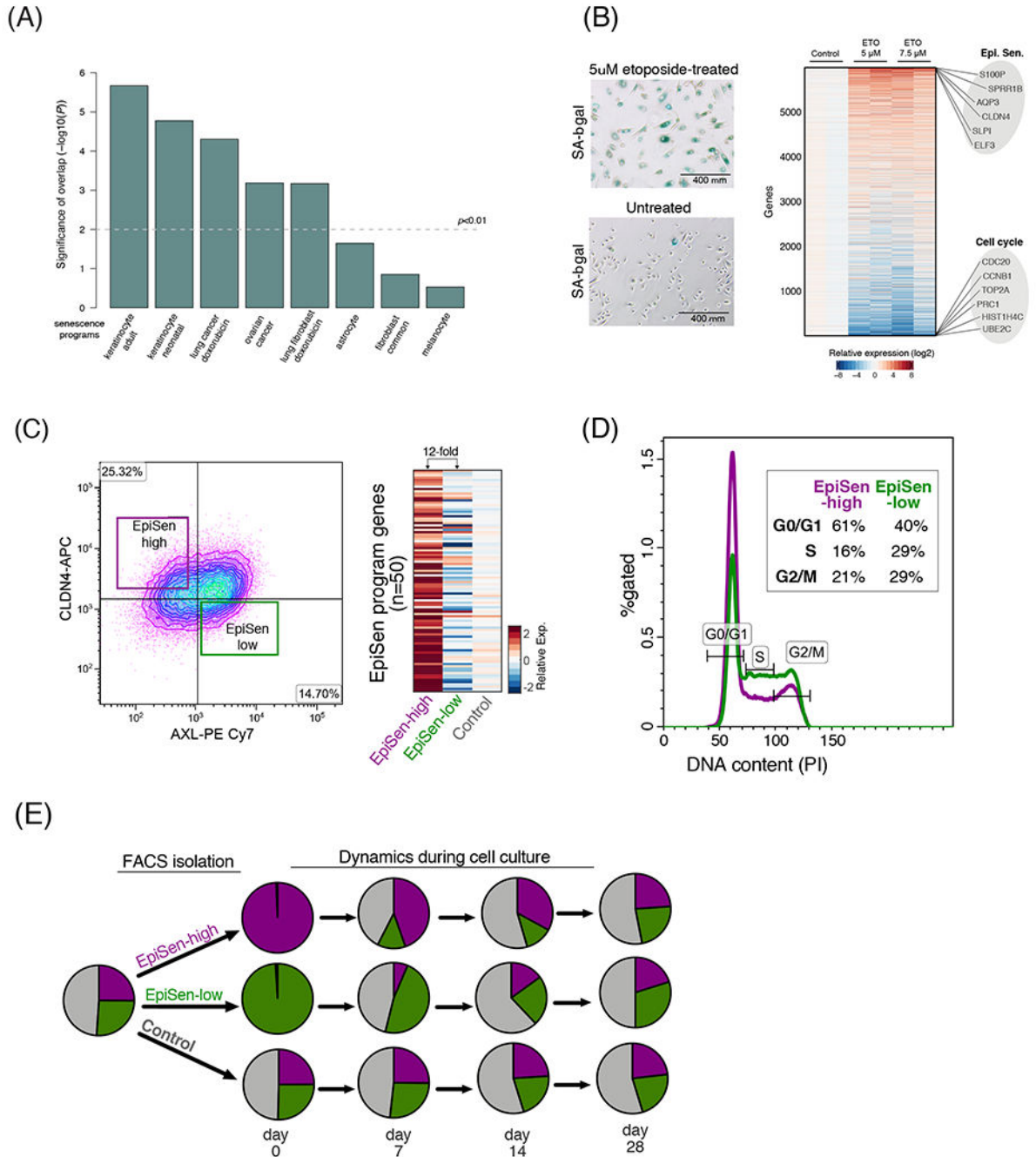


Figure 5. Interrogating the EpiSen RHP in primary cells and model cell lines.

(A) Significance of the overlap ($-\log_{10}(P)$, hypergeometric test) between the EpiSen RHP and eight previously reported senescence programs. (B) Left: induction of senescence by etoposide in primary lung bronchial cells confirmed by SA- β -gal staining. Right: heatmap depicts the relative expression of 6,000 genes (rows) in primary lung bronchial cells, 9 days after induction of senescence by etoposide treatment for 48h at two concentrations with 2 biological replicates. EpiSen and cell cycle programs were the most upregulated and downregulated programs, respectively (see fig. S5D); selected genes from these programs

are labeled. **(C)** Isolation of the EpiSen-high (AXL⁺ CLDN4⁻) and EpiSen-low (AXL⁺CLDN4⁻) populations by FACS in JHU006. Heatmap shows relative expression of the EpiSen program genes in three sorted subpopulations: two as shown at the right panel and a third control population. **(D)** FACS analysis of cell cycle by the DNA binding dye propidium iodide (PI) on sorted EpiSen-high and EpiSen-low cells in JHU006. **(E)** Pie charts depict relative proportions of the EpiSen-high and EpiSen-low subpopulations in SCC47, for an unsorted sample (left, initial distribution), and for sorted subpopulations that were analyzed immediately after sorting (day 0) and at three additional time points (at days 7, 14 and 28 in culture).

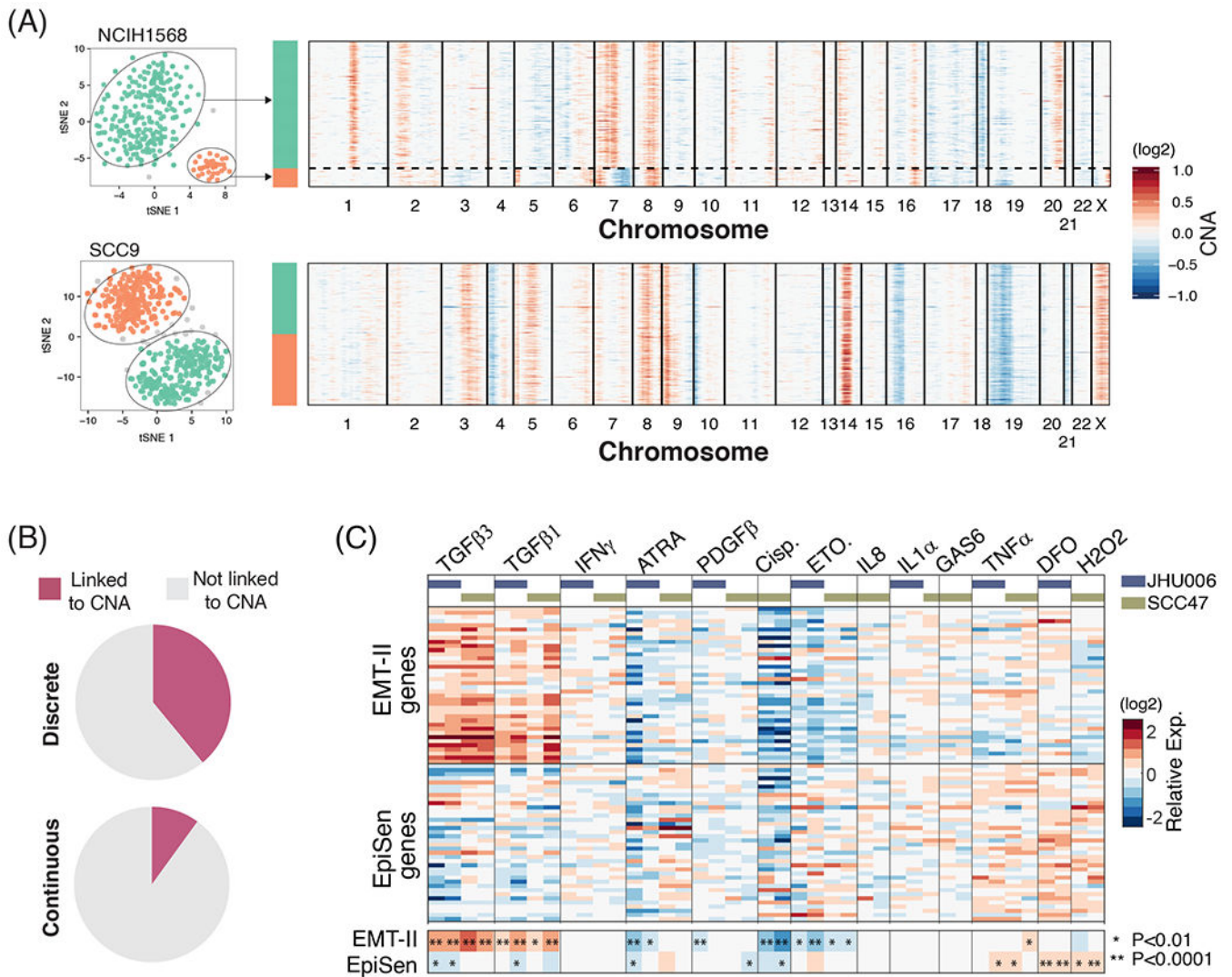


Figure 6. Genetic and microenvironmental factors partially explain expression heterogeneity. (A) Representative cell lines showing the association (top panel) or lack thereof (bottom panel) between discrete subpopulations and CNA-based subclones. t-SNE plots on the left show discrete subpopulations identified using DBSCAN (as in Fig. 2B and S1C). Heatmaps on the right depict inferred CNAs ordered according to the expression-based clusters. (B) Percentage of discrete (left) and continuous (right) heterogeneity programs that are associated with genetic subclones. For discrete programs, associations were assessed by comparing the assignment of cells to CNA subclones and to expression-based subpopulations ($P < 0.001$, Fisher's exact test); for continuous programs, we compared NMF cell scores between different clones ($P < 0.001$, t-test). (C) Main heatmap depicts relative expression of EpiSen program genes and EMT-II program genes following multiple perturbations in SCC47 and JHU006. Smaller heatmap at the bottom shows the average values for the EMT-II genes and EpiSen genes, and asterisks denote significant up or down-regulation (by t-test, P value indicated in figure).

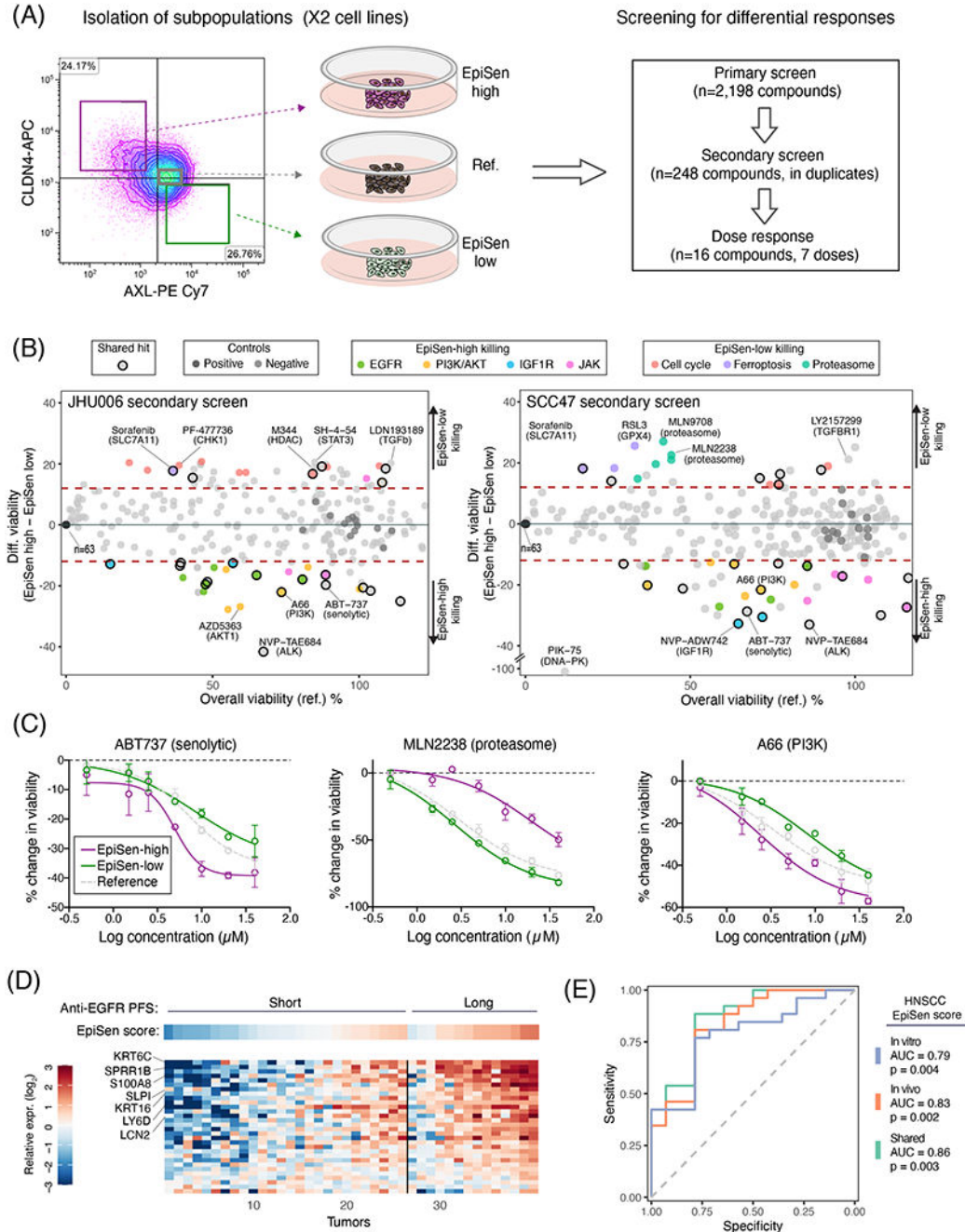


Figure 7. Co-existing cellular states differ in drug sensitivity.

(A) Experimental scheme for drug screening: three subpopulations were isolated by FACS and subjected to primary screen, secondary screen and dose response analysis of selected hits. (B) Viability of the reference population (X-axis) and differential viability of the EpiSen-high vs. EpiSen-low populations (Y-axis) upon treatment with 248 compounds tested in the secondary screen, in JHU006 (left) and SCC47 (right), averaged over 2 replicates. Dotted lines represent thresholds for differential sensitivity (as described in Methods). Selected hits and controls are colored by target as specified in the top legends. (C)

Dose response curves of three selected compounds in SCC47 measured in duplicate at each concentration, presented by the change in viability relative to vehicle controls. Error bars represent standard deviation. **(D)** Heatmap showing the expression of EpiSen genes shared between the HNSCC cell lines (*in vitro*) and tumors (*in vivo*) programs (see fig. S12) in bulk pre-treatment samples of 40 recurrent or metastatic HNSCC patients, stratified into short and long PFS following treatment with Cetuximab plus platinum-based chemotherapy. Top panel shows the corresponding EpiSen scores. Genes are ordered by differential expression ($\log_2(\text{fold change})$) comparing short and long PFS patients, and tumors are ordered within each group according to the EpiSen score. Selected genes are labeled. **(E)** Receiver operating characteristic (ROC) curves for prediction of long vs. short PFS patients following Cetuximab treatment. Curves depict the predictive power of three potential HNSCC EpiSen signatures (*in vitro*, *in vivo* and shared). P values were calculated for each signature separately using multivariate logistic regression correcting for relevant clinicopathological features.